Room temperature lasing unraveled by a strong resonance between gain and parasitic absorption in uniaxially strained germanium

Shashank Gupta, Donguk Nam, Jelena Vuckovic, and Krishna Saraswat

Phys. Rev. B **97**, 155127 — Published 13 April 2018

DOI: 10.1103/PhysRevB.97.155127

Room temperature lasing unraveled by a strong resonance between gain and parasitic absorption in uniaxially strained germanium

Shashank Gupta,[1,*] Donguk Nam,[2] Jelena Vuckovic,[1] and Krishna Saraswat[1]

[1] *Department of Electrical Engineering, Stanford University, Stanford, California 94305, United States*
[2] *School of Electrical and Electronic Engineering, Nanyang Technological University, Singapore*

A CMOS compatible on-chip light source is the holy grail of silicon photonics and has the potential to alleviate the key scaling issues arising due to electrical interconnects. Despite several theoretical predictions, a sustainable, room temperature laser from a group IV material is yet to be demonstrated. In this work, we show that a particular loss mechanism, inter-valence-band absorption (IVBA), has been inadequately modeled until now and capturing its effect accurately as a function of strain is crucial to understanding light emission processes from uniaxially strained germanium (Ge). We present a detailed model of light emission in Ge that accurately models IVBA in the presence of strain and other factors such as polarization, doping and carrier injection, thereby revising the roadmap towards a room temperature Ge laser. Strikingly, a special resonance between gain and loss mechanisms at 4-5% ⟨100⟩ uniaxial strain is found resulting in a high net-gain of more than $400cm^{-1}$ at room temperature. It is shown that achieving this resonance should be the goal of experimental work rather than pursuing a direct band-gap Ge.

I. INTRODUCTION

Silicon photonics is considered a key enabling technology for future CMOS systems since it has the potential to alleviate the bandwidth-power-density bottleneck of electrical interconnects[1]. Due to restrictive energy limits, this will require fully integrated on-chip optical interconnects[1,2]. A CMOS compatible light source is the only missing piece in the otherwise well integrated silicon photonics technology[1,2] and germanium (Ge) has garnered much interest due to its excellent CMOS compatibility[3–10]. Several approaches such as doping, strain and tin (Sn) alloying have been proposed[3–10] for lasing from Ge but a successful demonstration at room temperature is yet to be seen. Strain coupled with appropriate doping is a promising approach because it reduces the energy gap difference between direct and indirect bands, thereby increasing the electron population in the direct Γ valley which consequently leads to significantly lowered thresholds for lasing[3–8]. However, the parasitic free carrier absorption (FCA) in the valence bands, also known as inter-valence-band absorption (IVBA) has been experimentally and theoretically shown to incur so significant a loss that it nullifies any material gain achieved through strain and/or doping[11–14]. Despite the fact that IVBA is a major barrier to the realization of a room temperature group IV light source, there has been no major study which accurately models it and systematically captures the effect of strain on this parasitic absorption. Most of the modeling work to date assumes a simple closed form expression for IVBA which was obtained by a sparse fit of the measured absorption in relaxed Ge as in Ref. 3 or on slightly strained (0.2%) Ge as in Refs. 4 and 11. In this work, we instead model IVBA and the material gain of Ge under various amounts of uniaxial tensile strains using first principles. We show that the simple IVBA expression used in the bulk of published literature significantly deviates from the predictions of our rigorous model and that it does not capture the essential underlying physics particularly at high strain values. Using our model, we predict that positive net-gain from Ge can be achieved at room temperature only within a small window with uniaxial tensile strain between 4 and 5%. This striking result should encourage researchers to pursue the roadmap built in this work and demonstrate a room temperature Ge laser.

As illustrated in Fig.1(a), direct transitions from the top two valence bands (VB1 and VB2) to the lowest conduction band (CB1) are responsible for optical gain in Ge while the direct transitions from split-off band (SO) to VB1 and VB2 make up majority of the IVBA loss mechanism[11]. The Empirical Pseudopotential Method (EPM), discussed in Section II, is used to compute detailed band-structures of strained Ge (s-Ge) with the band-gaps corresponding to all relevant transitions shown in Fig.1(b) alongside the available experimental data[5,12,15,16]. It is evident that the relative band-gaps corresponding to the transitions change significantly with strain and hence any expression derived for relaxed Ge may not capture the correct physics for highly s-Ge.

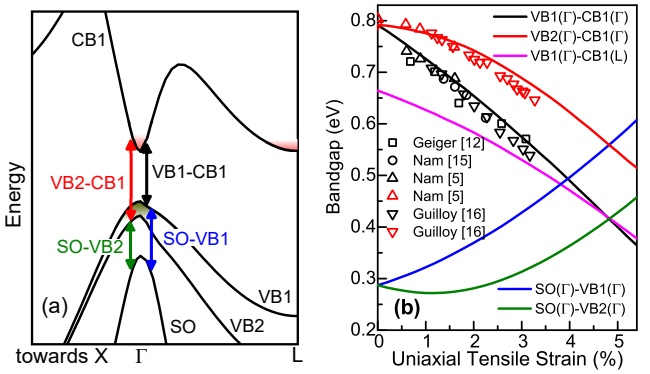

FIG. 1. (a) Band diagram of strained Ge indicating the main transitions in the light emission process, (b) Band-gap as a function of strain for different transitions along with the available experimental data.

For instance, consider the band-gap for VB1-CB1 (black curve in Fig.1(b)) and SO-VB1 (blue curve in Fig.1(b)) transitions. For bulk Ge, SO-VB1 band-gap is significantly smaller than VB1-CB1 and if the light emission occurs with photon energy approximately equal to VB1-CB1 band-gap, the probability that it will be absorbed by SO-VB1 transition will be relatively small. However, the band-gaps for those two transitions become equal (black and blue lines intersect) around 4% uniaxial strain. At this point the photons emitted due to the VB1-CB1 transition can be easily absorbed by the large number of allowed states corresponding to SO-VB1 transition. Section III will elaborate on this important resonance effect of strain on the gain and loss mechanisms. For s-Ge, the polarization of light becomes an important factor due to band-mixing effects in the valence band[5] and the momentum matrix elements that capture the polarization effects need to be accurately accounted for. Section IV deals with understanding these momentum matrix elements and the crucial role they play in the light emission process from s-Ge. Section V discusses the effect of carrier injection and doping and lays out a roadmap depicting suitable conditions that will lead to lasing from s-Ge at room temperature.

II. SIMULATION METHODOLOGY AND COMPARISON WITH EXPERIMENTS

We have employed the Empirical Pseudopotential Method (EPM) for calculating the band structures of unstrained and s-Ge. EPM allows us to compute a material's band structure using a relatively small number of empirical parameters. In the past, EPM has been used to describe the electronic properties of strained Si and Ge with remarkable success[17]. According to Chelikowsky and Cohen[18], the single electron Hamiltonian can be written as:

$$H(G,G') = -\frac{\hbar^2}{2m}\nabla^2 + V_{loc}(|G-G'|) + V_{nloc}(G,G') + V_{so}(G,G')$$

where V_{loc}, V_{nloc}, and V_{so} represent the local, nonlocal, and spin orbit contributions to the pseudopotential, respectively. We have used a basis set $\{G\}$ consisting of 169 plane waves to expand the pseudopotential in the reciprocal space. V_{loc} depends only on the magnitude of the reciprocal lattice vector $q = |G - G_0|$ and V_{nloc} captures the angular momentum dependence of the pseudopotential. For obtaining the band structure of pure unstrained material, the local pseudopotential form factors are required only at certain discrete values of reciprocal lattice vector given by $q^2 = \{0, 3, 8, 11\} * (2\pi/a_0)^2$. However, for band structure calculations of s-Ge, local pseudopotential at an arbitrary reciprocal vector q is needed and is obtained by performing cubic spline interpolation between local pseudopotential form factors V_{loc} at discrete q values mentioned above[19]. For the interpolation, the slope of the curve at those discrete q points is used as a variable. The slope of the curve determines, among other properties, the change in band-gaps with strain (a.k.a. deformation potentials) and therefore is a good choice to use as a parameter in the study of strained materials. Also, in order to ensure a fast cut-off at large q^2 we have followed the approach of Ref. 20 and required:

$$V_{loc}(q) = V_{cubic}(q)\left(\frac{1}{4}tanh\left(\frac{a_5 - q^2}{a_6}\right) + \frac{1}{4}\right)$$

We used analytical expressions as in Ref. 19 for overlap integrals $B_{nl}(K)$ needed for evaluation of the matrix elements for spin orbit interaction:

$$B_{nl}(K) = \frac{5 - (K/\zeta)^2}{5\left(1 + (K/\zeta)^2\right)^4}$$

Table I lists the values of pseudopotential parameters used for Ge. The pseudopotential parameters for nonlocal corrections have been slightly modified from those in Refs. 17 and 18 so as to reproduce as closely as possible the band structure of Ge from Ref. 18. Fig.2(a) and 2(b) show the calculated band structure of relaxed Ge and Ge with 5% uniaxial strain, respectively. The variation of band-gap with strain is shown in Fig.1(b) and the accurate matching of simulation data with different experiments demonstrates its credibility. As shown in table II, the band-gaps and effective masses from our simulations are in excellent agreement with those in Ref. 21. Compared to other notable reports on s-Ge light emission that use deformation potentials to account for strain[4,22,23], this work employs a more thorough treatment of s-Ge band structures.

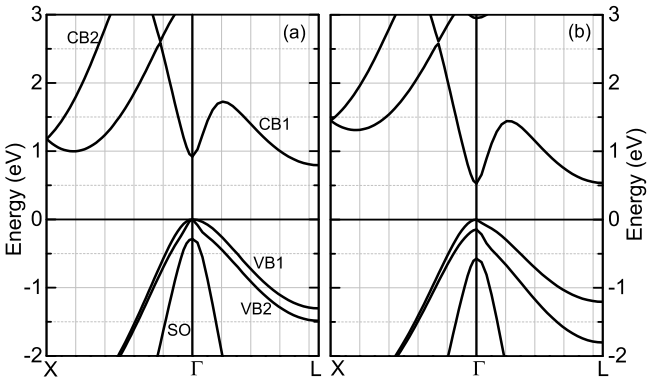

FIG. 2. Band diagrams computed using the empirical pseudopotential method for uniaxial strain (a) 0% i.e. bulk Ge and (b) 5%

After calculating the band structures, Fermi's Golden Rule is used in order to calculate the transition rates between different bands in Ge. The absorption (or gain when positive) due to band-to-band transitions is calculated using:

$$\alpha = C_0 \sum_k \delta(E_1(k) - E_2(k) - \hbar\omega) \times (f_1 - f_2) \times \mid \hat{e} \cdot p_{12}(k) \mid^2$$

where $C_0 = \pi e^2/cn\epsilon_0 m_0^2\omega$ is a constant.

TABLE I. EPM parameters used in this work

	Symbol	*Unit*	*Value*
Lattice constant	a	Å	5.658
Local form factor	V3	Ry	-0.236
	V8	Ry	0.019
	V11	Ry	0.056
Cubic spline interpolation slope parameters	S3	-	0.21
	S8	-	0.06
	S11	-	0.07
Pseudopotential cut-off parameters	a5	a.u.	4.5
	a6	a.u.	0.3
Spin-orbit parameters	ζ	$Å^{-1}$	10.09
	μ	Ry	0.0017
Elastic Constants	C11	GPa	128.53
	C12	GPa	48.62

The term $\delta(E_1(k) - E_2(k) - \hbar\omega)$ represents the joint density of states (JDoS) between bands 1 and 2 corresponding to direct transitions of energy $\hbar\omega$. It can be calculated directly from the band structure of the material by counting the number of states between band 1 and 2 with an energy difference equal to $\hbar\omega$. A constant lifetime broadening value of 20meV has been used in this work similar to other published reports.[22,24] $f_1 - f_2$ refers to the Fermi inversion factor. Each of f_1 and f_2 are Fermi functions which depend on the band structure, doping and injection conditions in the material. The quantity $\mid \hat{e} \cdot p_{12}(k) \mid^2$ is the momentum matrix element for a particular wave vector k and $\hat{e}$ is the polarization. Momentum matrix elements p_{12} depend on wave function overlap between band 1 and 2. The wave functions for each band are obtained as a part of band structure calculations done using EPM. The three quantities JDOS, Fermi inversion factor and momentum matrix elements are calculated at each point in the first Brillouin zone (FBZ) and their product is then summed throughout the FBZ to obtain the absorption spectrum. It should be noted that the only empiricism that enters the simulation methodology is through the pseudopotential of s-Ge. The rest of the methodology is based on first principles and there are no fitting parameters involved apart from the pseudopotential itself. Second order effects such as the energy band re-normalizations due to multiple particle effects are not considered in the present model and are out of scope of this work. Moreover, arguments made in Ref. 3 show that these second order effects will not impact the outcome of this work.

TABLE II. Band structure parameters compared with experiments from Ref. 21

Band-gap	$\Gamma_v - \Gamma_c$	$\Gamma_v - L_c$	Δ_{so}
This work	0.9214	0.7943	0.2871
Literature	0.928	0.79	0.29
Effective mass(e^-)	m_e^Γ	$m_{e,l}^L$	$m_{e,t}^L$
This work	0.047	1.58	0.093
Literature	0.049	1.568	0.094
Effective mass(h^+)	m_{HH}^{100}	m_{HH}^{110}	m_{LH}^{100}	m_{LH}^{110}
This work	0.248	0.466	0.059	0.054
Literature	0.254	0.477	0.049	0.056

As shown in Fig.3(a), the absorption spectrum of bulk Ge at 300K from our simulations matches the experimental data from Ref. 25 accurately. In this work, we have used the same formalism described above to calculate the IVBA as well. The absorption spectrum of bulk Ge below its band-gap taken from experimental data in Ref. 26 is shown in Fig.3(b). This absorption is because of the IVBA transitions previously described[11]. The simulation data matches accurately for a hole density of $6 \times 10^{15} cm^{-3}$ and two different temperatures. Different temperatures basically probe the correctness of Fermi functions used in the model and a good fit with experimental data proves the same. A comparison of experimental data from Ref. 27 with simulations for a hole density of $1.58 \times 10^{17} cm^{-3}$ is shown in Fig.3(c). The simulations agrees with the experiments reasonably well. It was seen that the agreement between simulations and experiments became worse for higher hole densities in Ge. This can be explained by the fact that the experimental data achieved the specific hole concentration through doping and at higher doping levels the p-dopant atoms start to play a role in absorption. The effect of p-

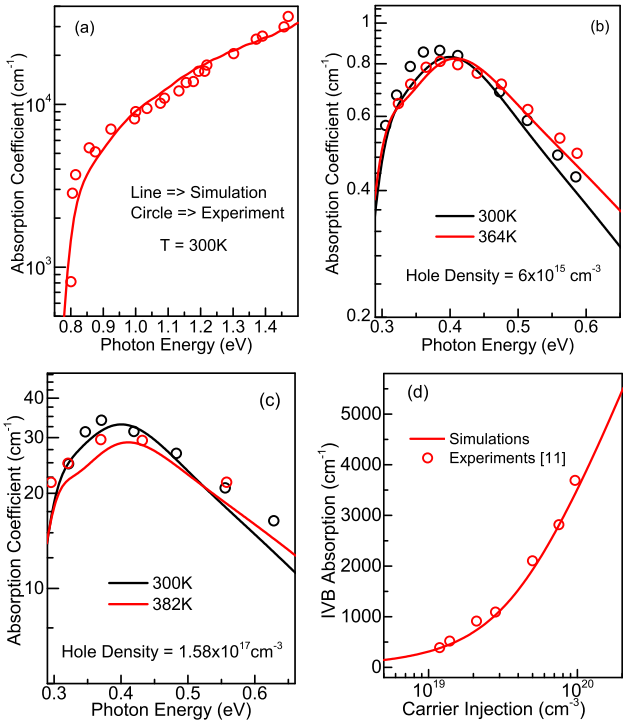

FIG. 3. (a) Computed absorption spectrum of Ge along with experiments from Ref. 25 at 300K, (b) Infrared absorption of Ge due to IVBA compared with experiments from Ref. 26, (c) Infrared absorption of Ge for hole density of $1.58 \times 10^{17} cm^{-3}$ and equivalent experimental data from Ref. 27 and (d) IVBA as a function of carrier injection compared with recent experiments from Ref. 11

dopant atoms on the absorption is explained by mixing of valence-band states due to charged impurity centers which are known to wash-out the features observed in the spectrum otherwise[28]. Nedeljkovic et al.[24] have fitted their model for high p-doping ($1 \times 10^{19} cm^{-3}$) using the same washed-out spectrum from Ref. 28 and hence they miss the extremums present in the spectrum without dopant impurity atoms. In case of s-Ge laser, holes are injected by means of optical or electrical excitation and not doping. As such, the effect of p-dopant atoms does not apply. In order to remove the artifacts from dopant atoms, we compare the simulations with experiments in Ref. 11 where high concentration of holes in Ge was achieved by carrier injection instead of p-doping. As shown in Fig.3(d), the match between the two is exceptional. The good fit of absorption spectrum in Ge with experimental data taken from different sources under different operating conditions instils complete confidence in the model developed. This work is unique in that we have used exactly the same basic formalism to describe all the transitions possible in this material system. In bulk of the other published work, the loss mechanism such as IVBA is captured by means of an over-simplified expression fitted for bulk Ge. In the next section, we show that the over-simplified expression does not capture the complete physics and leaves out essential pieces that are crucial to understanding the process.

III. EFFECT OF STRAIN ON GAIN AND INTER-VALENCE-BAND ABSORPTION

The formalism developed in section II is used to study the effect of strain on gain and IVBA. The band-to-band gain (denoted as just gain), shown as a function of photon energy and different strain values in Fig.4, is the sum of the gain obtained from transitions between VB1-CB1, VB2-CB1 and SO-CB1 bands. The gain curves are obtained for a doping of $2 \times 10^{19} cm^{-3}$ and a carrier injection level of $4 \times 10^{19} cm^{-3}$. The polarization of light is taken to be in a direction perpendicular to the strain axis. The effect of polarization, carrier injection and doping will be discussed in subsequent sections. Two important characteristics of the gain curve is that the peak gain increases with strain and it redshifts to lower photon energies. The peak gain increases primarily because Ge becomes more direct with increasing strain i.e. the energy gap between L and Γ valley in CB1 reduces with strain. The peak gain redshifts because the band-gap of Ge (between VB1 and CB1) reduces with strain. These two characteristics are well established both theoretically and experimentally[3–8] and our model captures them accurately.

IVBA as a function of photon energy and strain is shown in Fig 5. IVBA is the sum of absorption due to transitions between SO-VB1, SO-VB2 and VB2-VB1. The curves are computed for the same strain values, doping, injection and polarization as was used for gain calculations in Fig.4. The dashed curve in the figure is the closed form expression of IVBA fitted for Ge with a small biaxial strain of 0.15%[4,11] and is widely used in literature to compute IVBA for different strain values in Ge and completely different operating conditions. The IVBA from our model compares well with this closed form expression for the case of bulk Ge with emission wavelength close to 0.8eV. However, for a uniaxial strain of 4% and operating point close to 0.55eV (given by peak gain in Fig.4), our model predicts the IVBA to be $865 cm^{-1}$ whereas the expression from Refs. 4,11 gives $2161 cm^{-1}$, the difference between the two being $1296 cm^{-1}$. The closed form expression predicts a linear increase in IVBA with decreasing photon energy which is evidently not the case. As can be seen from the curves in Fig.5, there is a local maximum and a local minimum in IVBA and in order to understand these crucial extremes, Fig.6 separates the different components of IVBA for 3% uniaxial strain. SO-VB1 dominates the IVBA with VB2-VB1 transition playing an important role at lower photon energies. SO-VB2 transitions are limited because VB2 is mostly occupied at these injection levels making the number of allowed states for the transition very small. The local maximum corresponds to the increasing density of states (DoS) available for SO-VB1 transition limited by the Fermi function, which eventually dominates over increasing DoS and results in decaying IVBA beyond the maximum. The local minimum is because of lack of available states for transitions below SO-VB1 band-gap and

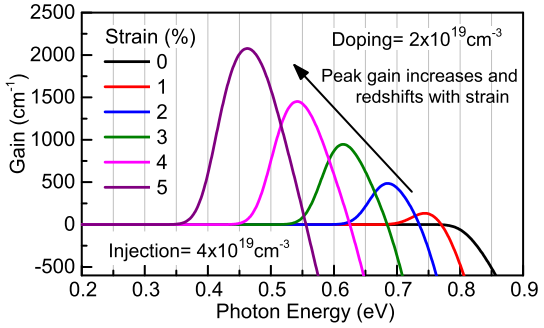

FIG. 4. Band-to-band gain as a function of photon energy and uniaxial strain. The doping and carrier injection is kept constant at $2 \times 10^{19} cm^{-3}$ and $4 \times 10^{19} cm^{-3}$ respectively.

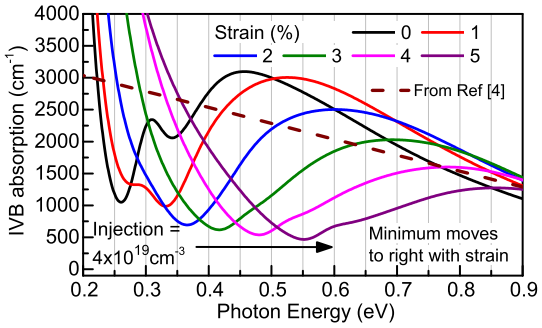

FIG. 5. IVBA as a function of photon energy and uniaxial strain for a carrier injection level of $4 \times 10^{19} cm^{-3}$. The dashed line shows the IVBA expression used in prior literature.

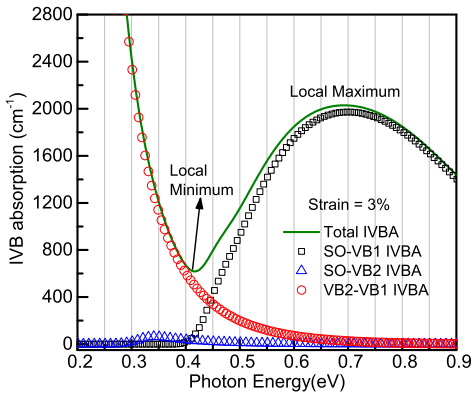

FIG. 6. The break-up of IVBA into different components for 3% strain in Ge.

limited by the allowed transitions between VB2 and VB1. Therefore, it is reasonable to conclude that the minimum in IVBA will occur at a photon energy which is approximately equal to the band-gap of SO-VB1 transition for a particular strain value. Since SO-VB1 band-gap increases significantly with strain (as shown in Fig.1(b)), the minimum in IVBA also shifts to higher photon energy with strain. As we apply strain to make the band-gap more direct, the Γ-VB1 separation shrinks and the SO-VB1 separation increases (shown in Fig.1b). This red-shifts the emission wavelength below 0.8eV (Fig.4) while simultaneously blue-shifting the parasitic IVBA curves (Fig.5). Fig.7 plots the gain and IVBA on the same energy scale to make it easily readable. It also shows the net-gain (Fig.7(c)) obtained after subtracting IVBA from the gain.

With increasing strain, the maximum of the parasitic IVBA spectrum is brought closer to the emission wavelength up to 3% strain (green curves in Fig.7) where the maximum in gain aligns with the IVBA maximum at 0.62eV. Critically, further increasing the strain brings the emission wavelength out of alignment with the IVBA maximum and into alignment with the IVBA minimum, starting at 4% strain (pink curves in Fig.7) where both the peak gain and IVBA minimum are close to 0.55 eV. This alignment remains until 5% strain beyond which IVBA increases rapidly due to VB2-VB1 transitions, thereby overwhelming any available gain. As a guide for the eye, we have extracted the maximum gain, IVBA at the wavelength of peak gain and the resulting net-gain from Fig.7 and plotted them in Fig.8. It can be seen that strain initially worsens the IVBA, a large and hitherto ignored effect. Thus, increasing the strain from 0 to 3% results in a modest increase in net gain, but further increasing the strain between 4 to 5% yields a dramatic increase in net gain. This is a newly identified resonance effect and is shown explicitly in Fig.7(c). Here, it should be emphasized that this resonance effect is independent of any modeling parameter artifact. This resonance occurs simply because CB1-VB1 bandgap intersects VB1-SO bandgap as a function of uniaxial strain (Fig. 1b). The actual value of strain at which this intersection takes

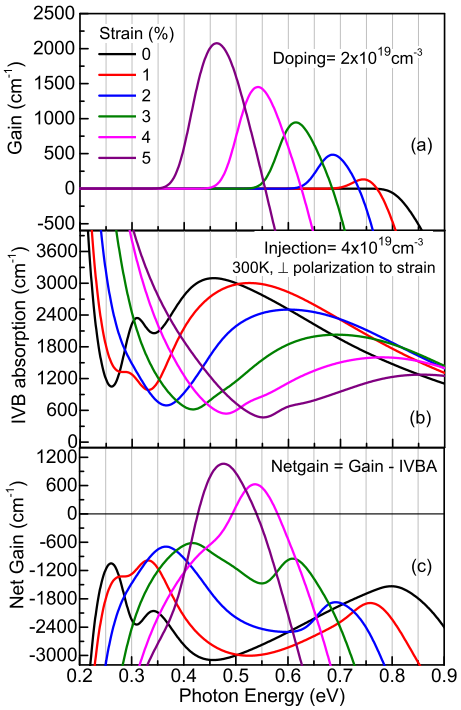

FIG. 7. (a) Band-to-band gain as a function of photon energy and strain (same as Fig.4), (b) IVBA on the same energy scale as gain and (c) Net-gain obtained after subtracting IVBA from gain.

place is subject to the modeling parameters used and after rigorous work, we found this value to be around 4%. On the contrary, the closed form expressions used in prior literature[3,4,22,23] are simple empirical fits that completely overlook this very critical resonance effect.

It should be noted that the net-gain up to this point was obtained by just subtracting IVBA from gain. One other loss mechanism that needs to be considered is the free carrier absorption due to electrons (eFCA) in the conduction band. The basic difference between eFCA and IVBA is that eFCA increases smoothly with decreasing photon energy and does not have maximum and minimum like features as was the case for IVBA[29]. This is because electrons cannot undergo vertical intra conduction-band transitions due to lack of available JDoS close to

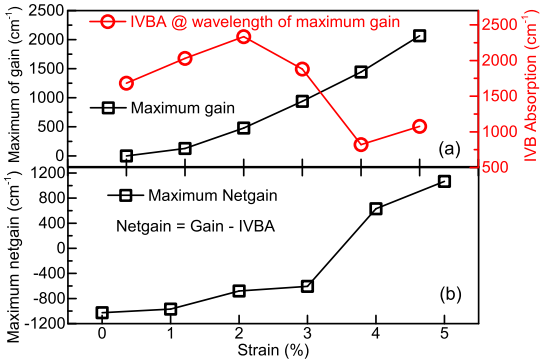

FIG. 8. (a) Maximum gain (left y-axis) and IVBA at the wavelength of maximum gain (right y-axis) extracted from Fig.7, (b) Maximum net-gain extracted from Fig.7(c).

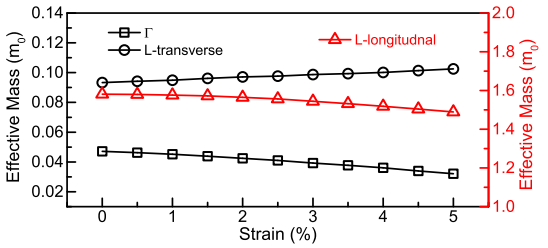

FIG. 9. Effective mass for Γ and L valley. Both longitudinal and transverse masses are shown for L valley.

emission photon energy[11]. It is well known that eFCA is based on a free electron effect i.e. the excited electron remains in the same energy band[29]. For free electrons to take part in intra-band absorption, conservation of momentum and conservation of energy both need to be satisfied which is only possible through phonon scattering and ionized impurity scattering[29]. Since eFCA occurs in the same energy band through interaction of photons, phonons and dopant impurities, it is valid to assume that it will only depend on the shape of that band (i.e. effective mass), temperature, doping and carrier injection. Fig.9 shows the effective mass of the Γ valley and L valley (both transverse and longitudinal mass) as a function of strain. It can be seen that the effective mass does not change appreciably in either valley as a function of strain. Therefore, for a given temperature, doping and carrier injection, eFCA can be expected to remain the same with strain. As such, an expression for eFCA fitted for bulk Ge[3] can be used for all strain values and the same has been used in this work. The net-gain after subtracting both IVBA and eFCA from gain is shown in Fig.10. For 4% strain, carrier injection of $4 \times 10^{19} cm^{-3}$ and doping of $2 \times 10^{19} cm^{-3}$, eFCA amounts to $744 cm^{-1}$ at peak gain and therefore reduces the net-gain from $627 cm^{-1}$ (Fig.4) to $-117 cm^{-1}$ (Fig.10). It can be seen that, under the above operating conditions, positive net-gain is available for uniaxial strain between 4 and 5% and only when the special resonance between gain and IVBA takes place. Detailed modeling of IVBA uncovered this resonance for the first time and holds the key for a room temperature Ge laser. Our findings strongly suggest that hitting this resonance should be the goal of experimental work around s-Ge whereas the pursuit of direct band-gap Ge has been the main objective thus far.

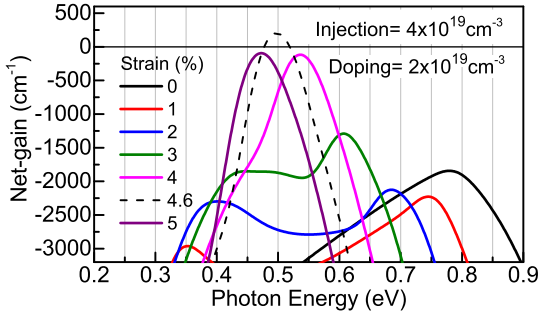

FIG. 10. Net-gain as a function of strain obtained after subtracting IVBA and eFCA from band-to-band gain.

IV. EFFECT OF POLARIZATION AND ROLE OF MOMENTUM MATRIX ELEMENTS

In section III, all the results were obtained for light polarized in a direction perpendicular to strain. The gain and IVBA for light polarized parallel to strain direction is shown in Fig.11. All the other simulation parameters are kept exactly the same as before. It is evident that there is no band-to-band gain available in this case which is remarkably different from the case when the light is polarized perpendicular to the strain as shown in Fig.4. It proves that the polarization of light plays an important role in the process of light emission which is also shown experimentally in Ref. 5. The shape of the IVBA curves is also significantly different between the two polarizations (compare Fig.11(b) and Fig.5). The effect of polarization is captured in the model by means of momentum matrix elements (MME) and since the effect is so large, it is imperative to study the matrix elements in detail. The matrix elements are calculated using the expression: $p_{12} = \langle \psi_1 \mid \hat{p} \mid \psi_2 \rangle$ where ψ_1 and ψ_2 are the wave-functions of the bands 1 and 2 and $\hat{p}$ is the momentum operator. The diagonalization of the EPM Hamiltonian described in Section II yields not only the energy levels (eigenvalues) but also the eigenvectors which are nothing but the wave-functions in the reciprocal space with the basis set G. The wave-functions are then converted into real-space by means of a simple transformation. After calculating the wave functions, p_{12} is obtained by performing the above operation. This computation is done for transition from band 1 to 2 at all points in the FBZ and so we obtain $p_{12}(k)$. It should be noted that the wave-functions computed using this methodology are not 'true' wave-functions since they miss the contribution of core states. However, it has been shown that these pseudo-wave-functions can be used to make important and novel conclusions regarding the optical properties of an excited semiconductor system.[18,30–32] Specifically, Ref. 31 demonstrates that the MME computed using EPM and the full orthogonalized-plane-wave method

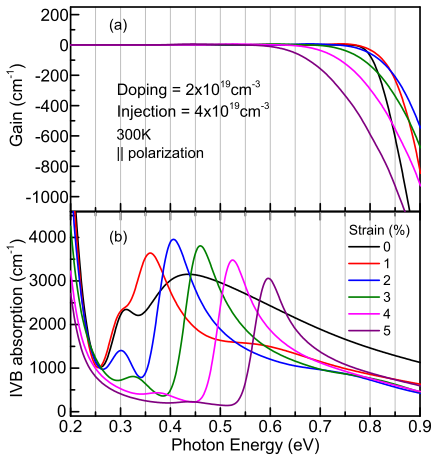

FIG. 11. (a) Gain and (b) IVBA for light polarized parallel to strain. No band to band gain is available in this case.

yield similar values.

The momentum matrix elements for the VB1-CB1 transition computed as a function of reciprocal space vectors (k) are shown in Fig.12. The Γ point is taken as the origin and then the k-vectors are plotted in the direction parallel to strain axis ([001]) on left side and in directions perpendicular to strain axis ([100] and [010]) on the right side. For the transition, we consider light polarized perpendicular to strain (left graph) and light polarized parallel to strain (right graph). It can be seen that for light polarized in [100] direction perpendicular to strain (Fig.12(a)), the momentum matrix elements are non-zero and large along [001] and [010] directions and tending towards zero only for [100] direction. When these matrix elements are introduced in the Fermi's Golden equation described before, it leads to a positive gain under certain conditions. On the contrary, for the light polarized in [001] direction parallel to strain (Fig.12(b)), the matrix elements tend to zero for all three axes except for bulk Ge. This is the precise reason which explains absence of gain in s-Ge when light is polarized parallel to strain. It also proves that strain significantly changes the valence band character due to mixing effects and it is necessary to compute these matrix elements as a function of strain. Using the same values for s-Ge as computed for bulk Ge will lead to erroneous results. The difference between the shapes of IVBA curves for different polarization of light is explained by the MME for SO-VB1 transition. Fig.13 shows the MME for SO-VB1 transition laid out in same way as Fig.12. On close examination, it can be observed that the matrix elements for perpendicular and parallel polarization of light are complementary to each other. For [100] polarization the elements tend to zero when they are maximum for the case of [001] light polarization. Because of the complementary nature, the shape of the IVBA curve is highly dependent on the polarization of the light. Therefore, from Fig.12 and 13 we can conclude that polarization of light plays a major role in underlying physics of light emission, more so, when valence band mixing effect takes place due to strain in the material.

Apart from the polarization of light, the dependence

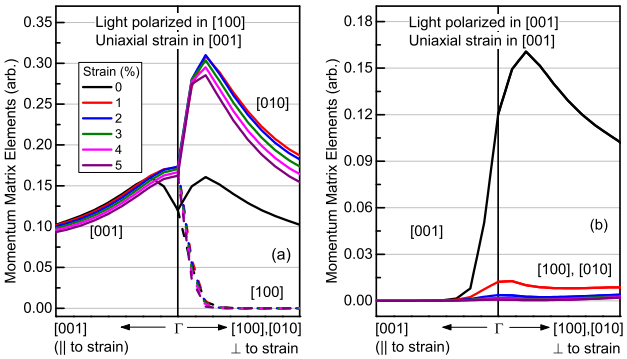

FIG. 12. Momentum matrix elements for VB1-CB1 transition; (a) Light polarized in [100] perpendicular to strain and (b) Light polarized in [001] parallel to strain.

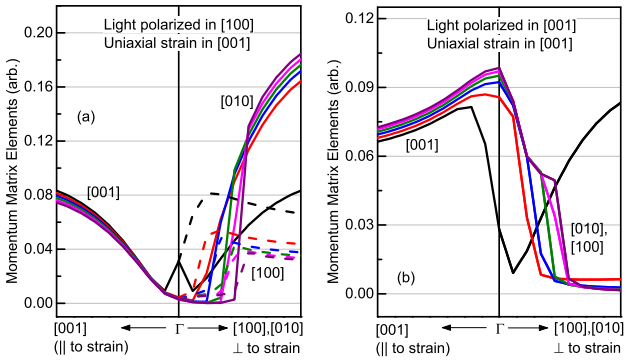

FIG. 13. Momentum matrix elements for SO-VB1 transition; (a) Light polarized in [100] perpendicular to strain and (b) Light polarized in [001] parallel to strain.

of matrix elements on k-vectors is also significant. The large variation in MME as a function of k-vectors can be established from Fig.13. In order to prove it further, Fig.14 compares the gain and IVBA for the case when the value at Γ (k=0) is used for all points while integrating over the FBZ in Fermis golden rule and for the case when the elements are evaluated separately for all k-points, which is the exact computation. Fig.14(a) compares the gain obtained for the two cases for the VB1-CB1 transition which is the major component of total gain. It is clear that the approximation of using MME at Γ for the complete FBZ is reasonable for gain calculation and it matches the exact computation well. This is because the MMEs for VB1-CB1 transition does not vary significantly over the FBZ and also because only the k-points very close to Γ actually contribute to the gain. The same approximation has been used for gain calculations in multiple other reports.[4,22,23,33] On the contrary, IVBA is remarkably different between the two cases for the SO-VB1 transition. This is because the MMEs change by more than an order of magnitude between Γ and the k-points close to Γ as shown in Fig.13(a). Moreover, with high injection levels required for achieving positive net-

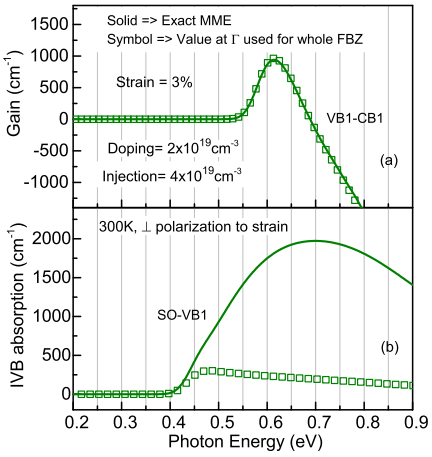

FIG. 14. Comparison of (a) gain and (b) IVBA for the case when momentum matrix elements at Γ is used for the complete FBZ and the case when the MME are evaluated separately at all points in FBZ which is the exact calculation.

gain, the fermi level can be expected to go deep into the valence bands and hence a large number of SO-VB1 transitions can take place away from the Γ point. Thus it is imperative to account for the change in MME for the SO-VB1 transition as a function of k-points in order to capture the IVBA accurately.

V. EFFECT OF CARRIER INJECTION AND DOPING

In the preceding sections the role of strain and polarization of light was studied while keeping the carrier injection fixed at $4 \times 10^{19} cm^{-3}$ and Ge doping at $2 \times 10^{19} cm^{-3}$. In this section, the effect of carrier injection and doping in Ge is studied in conjunction with uniaxial strain while assuming the polarization of light to be perpendicular to strain. The maximum net-gain as a function of both strain and carrier injection is shown in Fig.15 for undoped, $1 \times 10^{19} cm^{-3}$ and $5 \times 10^{19} cm^{-3}$ n-doped Ge. The desired area with a positive net-gain is demarcated with a bold black curve. It can be seen that positive net-gain is available only in a small window when the uniaxial strain is between 4-5%. For strain less than 4%, the band-to-band gain is very small because of the indirect band-gap of Ge. In addition, as discussed in Section III, at those strain levels the minimum in IVBA does not align with the maximum in gain thereby incurring large absorption loses. For strain greater than 5%, gain and IVBA begin to come out of alignment (as shown in Section III) and that again leads to large loses. It should also be noted that experimental demonstration of 4-5% uniaxial strain in Ge was done recently.[6]

Apart from strain, the carrier injection level required to get to positive net-gain depends on n-doping in Ge. N-type doping is useful in filling up the satellite L valley without adding unwanted holes in the valence band. Thus, higher the n-doping, lower is the carrier injection required to achieve transparency (net-gain equals zero). As shown in Fig.15, for undoped Ge, a minimum carrier injection of $3 \times 10^{19} cm^{-3}$ is required to achieve transparency while for a doping of $5 \times 10^{19} cm^{-3}$, this requirement drops to $1 \times 10^{19} cm^{-3}$. Moreover, the window in which the net-gain is positive becomes larger with increasing doping as well. However, there is an optimal n-doping for a given strain and adding more extrinsic electrons would then only result in more recombination and increased eFCA[34,35]. Therefore, it is evident that strain, carrier injection and doping have a strong interplay and all of them together play a central role in determining the light emission characteristics of uniaxially s-Ge.

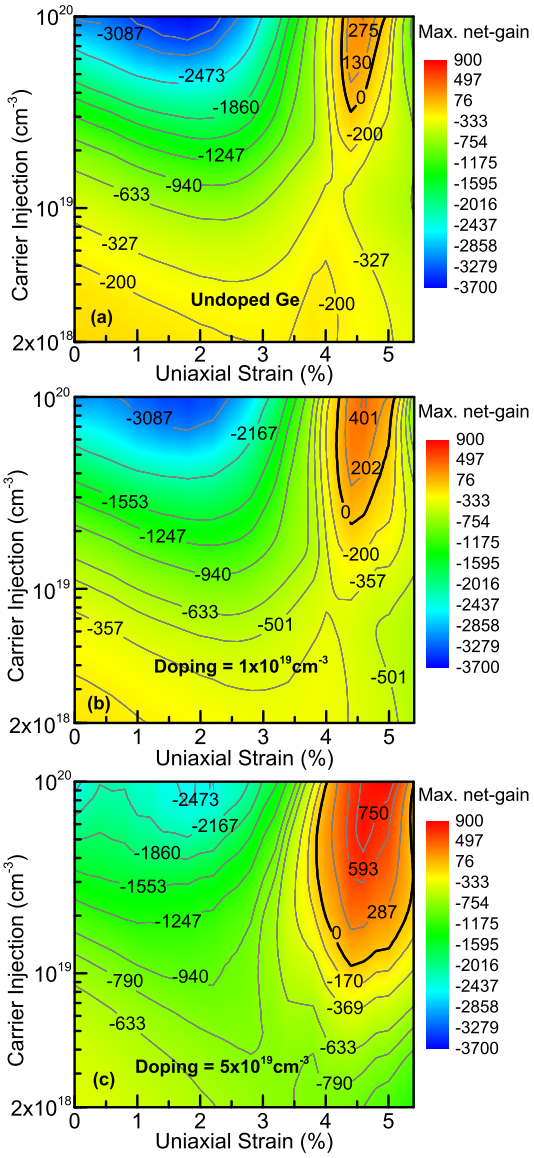

FIG. 15. Contour plots showing maximum net-gain as a function of strain and carrier injection. Ge is (a) undoped, (b) n-doped $1 \times 10^{19} cm^{-3}$ and (c) n-doped $5 \times 10^{19} cm^{-3}$. Positive net-gain is achievable in a narrow window between 4-5% strain.

VI. CONCLUSION

We have demonstrated that a detailed analysis of IVBA is necessary to correctly understand the loss mechanisms in s-Ge. The simple expression derived by fitting the experimental data for loss in bulk Ge is not sufficient and cannot be extrapolated to s-Ge. Our model ascertains that a positive net-gain can be achieved only when the maximum in band-to-band gain aligns with the minimum in the IVBA. This condition is predicted to occur for uniaxial strain between 4 and 5%. Notably, the requirement of direct band-gap material for positive net-gain is shown to be unnecessary at room temperature. The impact of strain on the MME due to valence band mixing is shown to be important. It is also mandatory to consider the MME as a function of reciprocal wavevectors (k) while calculating IVBA. Apart from strain, parameters such as polarization, carrier injection and

doping all play a key role in the carrier statistics of s-Ge. The model shows that the interaction between strain and parasitic absorption processes is critically important for the lasing process in tensile strained Ge. This substantially revises prior literature and builds a roadmap for a room temperature Ge light source.

ACKNOWLEDGMENTS

The authors would like to thank Dave Sukhdeo and Tomas Sarmiento for expert technical assistance and illuminating discussions. This work was supported by AFOSR for Si Compatible Electrically Pumped Direct Bandgap Ge/GeSn Laser (Grant number: FA9550-15-1-0388)

* sgupta14@stanford.edu

[1] D. Miller, Proceedings of the IEEE **97**, 1166 (2009).
[2] M. J. R. Heck and J. E. Bowers, IEEE Journal of Selected Topics in Quantum Electronics **20**, 332 (2014).
[3] J. Liu, X. Sun, D. Pan, X. Wang, L. C. Kimerling, T. L. Koch, and J. Michel, Optics Express **15**, 11272 (2007).
[4] M. J. Süess, R. Geiger, R. A. Minamisawa, G. Schiefler, J. Frigerio, D. Chrastina, G. Isella, R. Spolenak, J. Faist, and H. Sigg, Nature Photonics **7**, 466 (2013).
[5] D. Nam, D. S. Sukhdeo, S. Gupta, J. H. Kang, M. L. Brongersma, and K. C. Saraswat, IEEE Journal of Selected Topics in Quantum Electronics **20**, 16 (2014).
[6] D. S. Sukhdeo, D. Nam, J.-H. Kang, M. L. Brongersma, and K. C. Saraswat, Photonics Research **2**, A8 (2014).
[7] S. Gupta, D. Nam, J. Petykiewicz, D. Sukhdeo, J. Vuckovic, and K. Saraswat, in *2015 Conference on Lasers and Electro-Optics (CLEO)* (2015) pp. 1–2.
[8] A. Gassenq, K. Guilloy, G. O. Dias, N. Pauc, D. Rouchon, J.-M. Hartmann, J. Widiez, S. Tardif, F. Rieutord, J. Escalante, I. Duchemin, Y.-M. Niquet, R. Geiger, T. Zabel, H. Sigg, J. Faist, A. Chelnokov, V. Reboud, and V. Calvo, Applied Physics Letters **107**, 191904 (2015).
[9] S. Wirths, R. Geiger, N. V. D. Driesch, G. Mussler, T. Stoica, S. Mantl, Z. Ikonic, M. Luysberg, S. Chiussi, J. M. Hartmann, H. Sigg, J. Faist, D. Buca, and D. Grützmacher, Nature Photonics **9**, 88 (2015).
[10] D. Stange, S. Wirths, R. Geiger, C. Schulte-Braucks, B. Marzban, N. von den Driesch, G. Mussler, T. Zabel, T. Stoica, J.-M. Hartmann, S. Mantl, Z. Ikonic, D. Grtzmacher, H. Sigg, J. Witzens, and D. Buca, ACS Photonics **3**, 1279 (2016).
[11] L. Carroll, P. Friedli, S. Neuenschwander, H. Sigg, S. Cecchi, F. Isa, D. Chrastina, G. Isella, Y. Fedoryshyn, and J. Faist, Physical Review Letters **109**, 057402 (2012).
[12] R. Geiger, T. Zabel, and H. Sigg, Frontiers in Materials **2**, 52 (2015).
[13] J. Petykiewicz, D. Nam, D. S. Sukhdeo, S. Gupta, S. Buckley, A. Y. Piggott, J. Vuckovic, and K. C. Saraswat, Nano Letters **16**, 2168 (2016).
[14] H. Wen and E. Bellotti, Physical Review B **91**, 035307 (2015).
[15] D. Nam, D. S. Sukhdeo, J.-H. Kang, J. Petykiewicz, J. H. Lee, W. S. Jung, J. Vučković, M. L. Brongersma, and K. C. Saraswat, Nano letters **13**, 3118 (2013).
[16] K. Guilloy, N. Pauc, A. Gassenq, Y.-M. Niquet, J.-M. Escalante, I. Duchemin, S. Tardif, G. Osvaldo Dias, D. Rouchon, J. Widiez, J.-M. Hartmann, R. Geiger, T. Zabel, H. Sigg, J. Faist, A. Chelnokov, V. Reboud, and V. Calvo, ACS Photonics **3**, 1907 (2016).
[17] M. V. Fischetti and S. E. Laux, Journal of Applied Physics **80**, 2234 (1996).
[18] J. Chelikowsky and M. Cohen, Physical Review B **14**, 556 (1976).
[19] M. M. Rieger and P. Vogl, Physical Review B **48**, 14276 (1993).
[20] P. Friedel, M. S. Hybertsen, and M. Schlüter, Physical Review B **39**, 7974 (1989).
[21] M. V. Fischetti and J. M. Higman, "Theory and calculation of the deformation potential electron-phonon scattering rates in semiconductors," in *Monte Carlo Device Simulation: Full Band and Beyond*, edited by K. Hess (Springer US, Boston, MA, 1991) pp. 123–160.
[22] M. E. Kurdi, G. Fishman, S. Sauvage, and P. Boucaud, Journal of Applied Physics **107**, 013710 (2010).
[23] M. Virgilio, C. L. Manganelli, G. Grosso, G. Pizzi, and G. Capellini, Phys. Rev. B **87**, 235313 (2013).
[24] M. Nedeljkovic, R. Soref, and G. Z. Mashanovich, IEEE Photonics Journal **7**, 1 (2015).
[25] W. C. Dash and R. Newman, Physical Review **99**, 1151 (1955).
[26] H. B. Briggs and R. C. Fletcher, Physical Review **91**, 1342 (1953).
[27] W. Kaiser, R. J. Collins, and H. Y. Fan, Physical Review **91**, 1380 (1953).
[28] R. Newman and W. W. Tyler, Physical Review **105**, 885 (1957).
[29] H. Y. Fan, W. Spitzer, and R. J. Collins, Physical Review **101**, 566 (1956).
[30] J. P. Walter and M. L. Cohen, Phys. Rev. **183**, 763 (1969).
[31] J. P. Van Dyke, Physical Review B **5**, 1489 (1972).
[32] M. L. Cohen and J. R. Chelikowsky, *Electronic Structure and Optical Properties of Semiconductors* (Springer, Berlin, Heidelberg, 1988) p. 264.
[33] S. Gupta, J. Petykiewicz, D. Nam, D. Sukhdeo, J. Vuckovic, and K. Saraswat, in *2016 Conference on Lasers and Electro-Optics (CLEO)* (2016) pp. 1–2.
[34] B. Dutt, D. S. Sukhdeo, D. Nam, B. M. Vulovic, Z. Yuan, and K. C. Saraswat, IEEE Photonics Journal **4**, 2002 (2012).
[35] D. Sukhdeo, D. Nam, Z. Yuan, B. R. Dutt, and K. C. Saraswat, in *CLEO: 2013* (Optical Society of America, 2013) p. JTh2A.109.